Effect of concomitant elements on the distribution of ions in inductively coupled plasma mass spectrometry – Part 2: Polyatomic ions

ARTICLE *in* SPECTROCHIMICA ACTA PART B ATOMIC SPECTROSCOPY · DECEMBER 2001

Impact Factor: 3.18 · DOI: 10.1016/S0584-8547(01)00346-9

2 AUTHORS, INCLUDING:

Diane Beauchemin
Queen's University
125 PUBLICATIONS **3,014** CITATIONS

ELSEVIER

Spectrochimica Acta Part B 56 (2001) 2479–2495

SPECTROCHIMICA ACTA PART B

www.elsevier.com/locate/sab

Effect of concomitant elements on the distribution of ions in inductively coupled plasma mass spectrometry — part 2: polyatomic ions

Matheson M. Fraser, Diane Beauchemin*

Queen's University, Department of Chemistry, Kingston, Ontario, Canada, K7L 3N6

Received 11 August 2000; accepted 30 August 2001

Abstract

The effect of various concomitant elements in inductively coupled plasma mass spectrometry (ICP-MS) was assessed by measuring the distribution of selected polyatomic singly-charged ions, i.e. oxides of selected analytes (LaO^+ and CeO^+) as well as some background ions (Ar_2^+, ArO^+ and CO_2^+), in the plasma. This was accomplished while moving the ICP across and away from the sampling interface with or without a single concomitant element. This study included concomitant elements that were similar in ionization potential, but different in mass (Na, K, Cs and Cl, I), as well as similar in mass but different in ionization potential (K and Cl, Cs and I). Space–charge effects were dominant in many cases. However, the axial profiles of the $LaO^+/(La^+ + LaO^+)$ ratio, which should be fairly independent of such effects, were only affected by easily ionized elements (E.I.E.s), i.e. alkalis. A shift of the whole axial profile to lower height A.L.C. was observed in the presence of 0.02 M K or Cs, which is strong evidence for earlier desolvation. However, no shift was observed with 0.02 M Na, where the profile was only suppressed at low heights A.L.C., where the electron density would be most affected. This is consistent with a shift in ionization equilibrium. Further evidence for the latter was observed in the Ar_2^+ axial profiles, which were shifted to greater height A.L.C. in the presence of E.I.E.s. Finally, CO_2^+ was found to behave like the analyte oxides and the analytes, in contrast to ArO^+. This implies that CO_2^+ originates from dissolved carbon dioxide in the sample.

Keywords: Inductively coupled plasma mass spectrometry (ICP-MS); Matrix effects; Easily ionized elements; Spatial profiling; Space-charge effects; Ion-atom equilibrium; Ambipolar diffusion

* Corresponding author.
E-mail address: beauchmn@chem.queensu.ca (D. Beauchemin).

0584-8547/01/$ - see front matter
PII: S0584-8547(01)00346-9

1. Introduction

In Part 1 of this work [1], a study of the effect of individual concomitant elements (Na, K, Cs, Cl and I) on numerous analytes, covering a wide range of mass and ionization potential, was conducted. This was done in an attempt to elucidate the mechanisms involved in the suppressions and/or enhancements that have been reported previously in inductively coupled plasma mass spectrometry (ICP-MS). One reason for the wide range of effects observed in the literature with a given matrix element was found to be the age of the sampling interface, which was demonstrated to change the relative locations within the plasma where suppressions and enhancements occur [1].

Axial and radial profiles of the analyte distribution, with and without a concomitant element, revealed that space–charge effects were the predominant mechanisms involved in suppression [1]. However, there was also evidence of ambipolar diffusion low in the plasma. The observed broadening, which appeared to be more significant for doubly-ionized elements, increased with decreasing matrix element ionization energy but was independent of matrix or analyte element masses [1].

Evidence of a shift in ionization equilibrium towards the atom was also reported [1]. Indeed, the degree of suppression of the analytes was dependent upon the first ionization potential of the matrix elements: for two matrix elements of similar mass, the suppression was significantly greater with the matrix element having the lowest ionization potential. Others have also reported that matrix elements having the lowest first ionization potential caused the greatest amount of suppression [2,3]. Furthermore, a 0.02 M Na matrix, which should contribute negligible space-charge effects, still resulted in an average suppression of $38 \pm 7\%$ (over all of the analytes) low in the plasma [1]. The extent of this suppression was too large to be attributed to a shift in the profile as a result of an earlier desolvation in presence of Na. Lazar and Farnsworth [4] have indeed reported that matrix-containing droplets could evaporate sooner than equal-size matrix-free droplets simply because the former contained less solvent. Xu et al. [5,6] have reported a shift towards smaller droplet radius in the droplet size distribution of the tertiary aerosol produced by pneumatic nebulization in the presence of dissolved solids as a result of aerosol static electrification, which would also result in earlier desolvation. In any case, only 4% of the suppression could be attributed to a shift in the profile as a result of an earlier desolvation [1].

The suppression observed with 0.02 M Na actually supports measurements made using Thompson and Rayleigh scattering [7] where a significant increase in electron density was noticed along the central axis of the plasma in the presence of an easily ionized element (EIE) such as the alkalis. Furthermore, the suppression being most important low in the plasma, is commensurate with the localized increase in electron density originating from an aerosol droplet containing an EIE (vs. a droplet free of EIE), which could shift the ionization equilibrium back toward the atomic form. This effect is indeed expected to be most significant low in the plasma where the temperature is cooler.

In this part of the study, more evidence for the various mechanisms will be sought by looking at the effect of the same concomitant elements on selected polyatomic ions. In particular, the fraction $MO^+/(M^+ + MO^+)$ of analyte oxide ions (i.e. where M is either La or Ce) will be considered to check for further evidence of a shift in ionization equilibrium. Indeed, Tanner [8] demonstrated that the oxide fraction $MO^+/(M^+ + MO^+)$ was a good reference point within the plasma because it could not be shifted by changes in lens potentials and plasma conditions (including a secondary discharge). This ratio may therefore be a sensitive indicator of shifts within the plasma. For instance, a change in the ion–atom equilibrium would be expected to change the axial profile observed for this ratio whereas space-charge effects within the MS would not. Tanner's observation [8] also provides evidence that the oxide ions are produced within the plasma, and not during sampling downstream of the sampler orifice. Although oxide formation is unlikely at the calculated plasma temperatures [9], the inhomogeneous distribution of droplets

(in terms of size) in the plasma may allow an analyte to react with oxygen from a nearby desolvating droplet [10,11]. This is supported by the decrease in excitation and Doppler temperatures, which was observed under conditions favoring oxide formation [12]. Furthermore, Tanner [13] reported that the kinetic energy of analyte oxide ions was smaller than that of the corresponding analyte ions which translated into the analyte oxide ions originating from a 761-K cooler plasma region than the analyte ions. Some axial profiles of the plasma have shown that the maximum of LaO^+ appears first in the plasma, that of La^+ being observed some 6 mm deeper into the plasma [12]. The signal maxima for $BaOH^+$, BaO^+, Ba^+ and Ba^{2+} were seen in that order when the plasma was moved away from the interface [14]. If the oxide signal originated solely from the

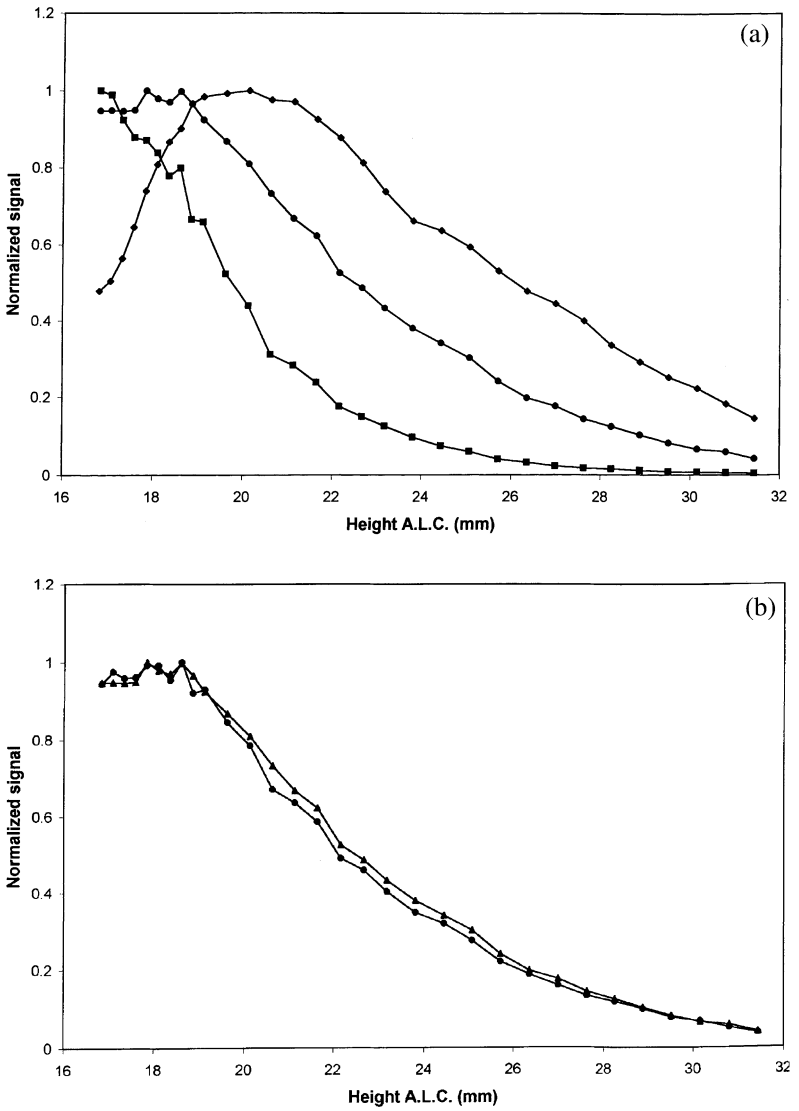

Fig. 1. Axial profiles of the normalized signals from a 100-μg/l solution in 1% HNO_3: (a) La^+ (losanges), Pb^+ (circles) and LaO^+ (squares); and (b) Pb^+ (triangles) and the sum of La^+ and LaO^+ (circles).

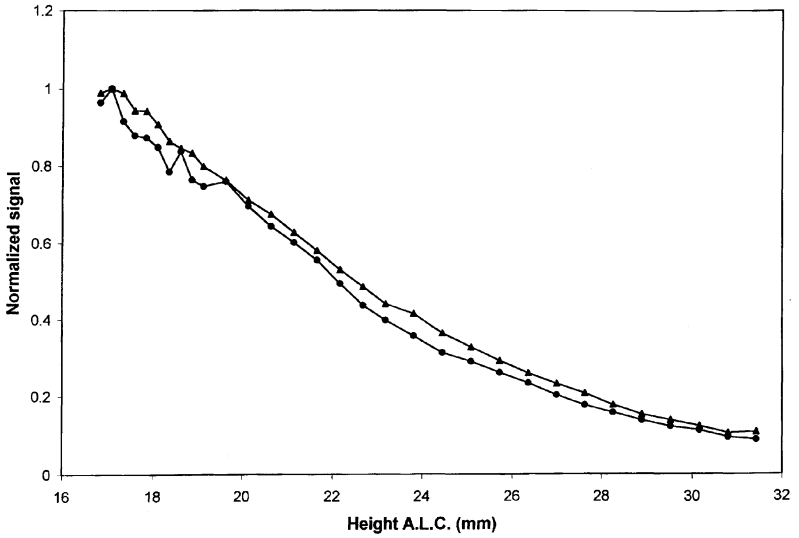

Fig. 2. Axial profiles of the normalized signals of Pb^+ (triangles) and the sum of La^+ and LaO^+ (circles) from a 100-μg/l solution in 0.02 M Na.

boundary layer, it would either appear at a greater height A.L.C. than the corresponding analyte signal, or be independent of the sampling position.

To further differentiate effects occurring downstream of the plasma from those taking place within, ArO^+, Ar_2^+ and CO_2^+ will also be monitored. The first ion is not expected to exist in the plasma because it is a weakly bound polyatomic ion species [15]. In fact, measurements of electron number density and rotational temperature in a secondary discharge were consistent with a collision-induced reaction of Ar with X^+ (where $X =$ C, N, O or Cl) in the interface region [16]. In contrast, calculations have shown that Ar_2^+ can be formed in the ICP through the combination reaction of Ar with Ar^+ [17]. In fact, even under 'cold plasma' conditions, Ar_2^+ persists (which is not the case of ArO^+ since these plasma conditions are used to allow the determination of Fe at m/z 56) [18]. Finally, a significant portion of CO_2^+ is expected to originate from dissolved carbon dioxide in the solutions. Indeed, with a solubility constant of 0.0344 [19] and an estimated 360 μatm CO_2 in the air [20], the concentration of dissolved CO_2 should be 12 μM. This concentration is similar or larger than those of the analytes in this study (for instance, 100 μg/l V corresponds to 2 μM). Assuming that the oxide bond strength of polyatomic ions follows the same order as their corresponding neutral diatomic molecules, CO_2 could survive the plasma since its oxide bond strength is greater than that of LaO and CeO. It would therefore, be expected to behave like these oxide ions, whereas ArO^+ should behave differently.

2. Experimental

2.1. Instrumental conditions

A Perkin–Elmer/SCIEX ELAN 500 ICP-MS

Table 1
Nebulization efficiency in presence of different matrices

Matrix	Nebulization efficiency (%)
1% HNO_3	2.81 ± 0.06[a]
1% HNO_3 + 0.02 M $NaNO_3$	2.91 ± 0.06
1% HNO_3 + 0.02 M KNO_3	2.68 ± 0.05
1% HNO_3 + 0.02 M $CsNO_3$	2.72 ± 0.04
1% HNO_3 + 0.02 M HCl	2.74 ± 0.06
1% HNO_3 + 0.02 M HI	2.71 ± 0.06

[a]All errors expressed as 95% confidence limits ($n = 8$–12).

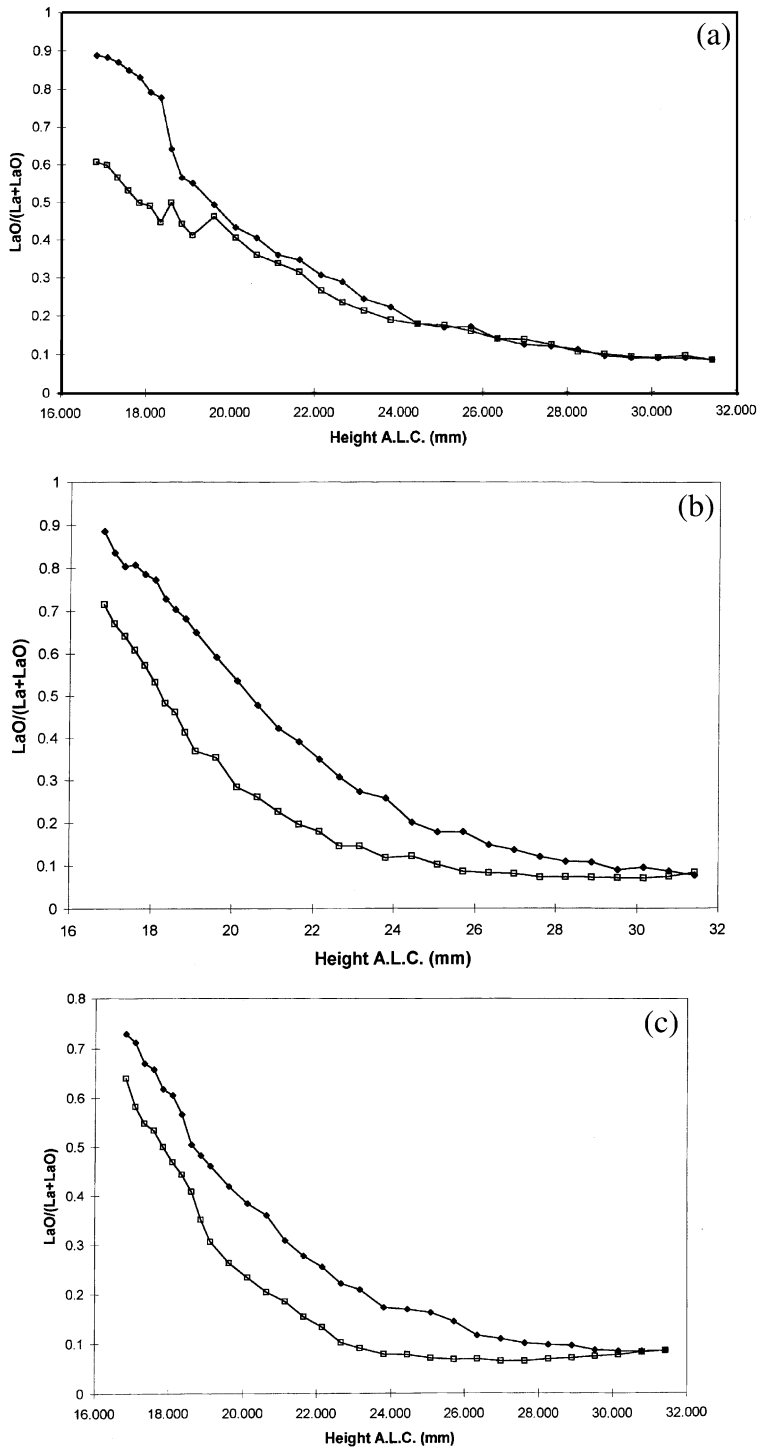

Fig. 3. Axial profiles of the normalized ratio of LaO^+ over the sum of La^+ and LaO^+ from a 100-μg/l solution in 1% HNO_3 (losanges) and a 0.02 M matrix (open squares) of: (a) Na; (b) K; (c) Cs; (d) Cl and (e) I.

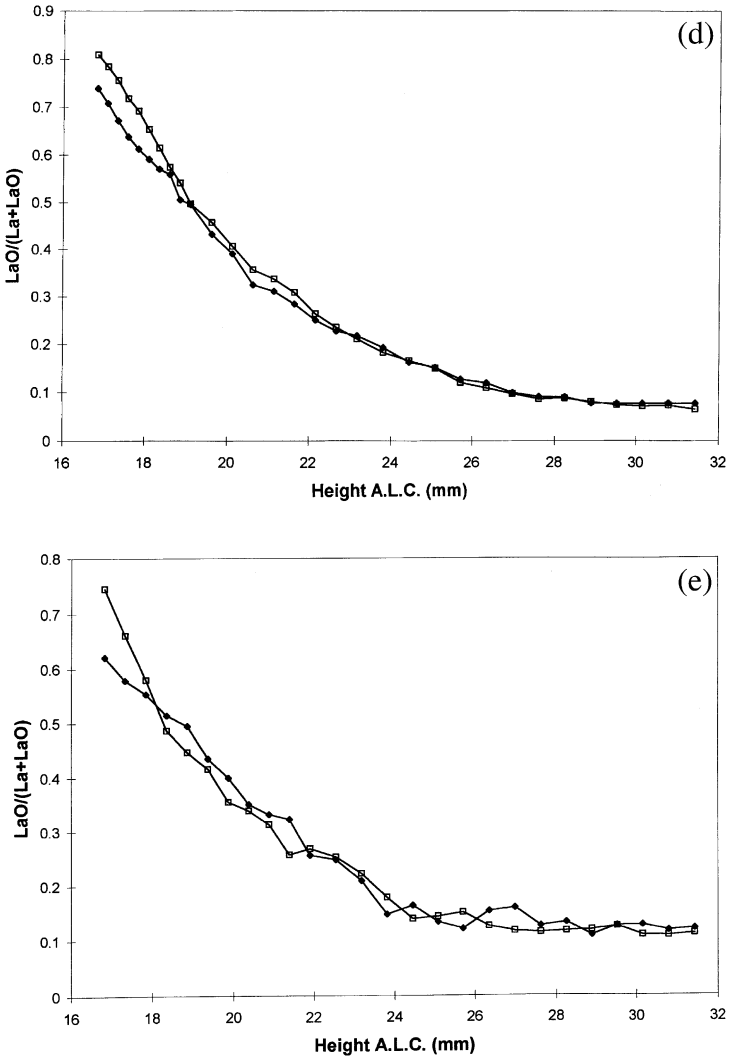

Fig. 3. (*Continued*).

instrument was used with several modifications that were described in Part 1 [1]. The operating conditions and optimization of the ICP-MS instrument are also identical to those in Part 1 [1]. The sample introduction system (i.e. Meinhard type-C nebulizer and Scott double-pass spray chamber) was kept constant throughout this study (as well as Part 1) to minimize effects arising from substantial changes in nebulization efficiency, residence time, etc. [21].

2.2. Reagents

A 100 μg l^{-1} multielement solution in 1% HNO_3 was prepared using high-purity HNO_3 (Ultrex II from J. T. Baker Inc., Phillipsburg, NJ, USA), 1000 g ml^{-1} monoelement standard solutions of the analyte nitrate or oxide (Plasma Standard from SPEX Industries, Edison, NJ, USA), ceric ammonium nitrate salt (Fisher Scientific, Fairlawn, NJ, USA) and deionized distilled water

(Milli-Q Plus System, Millipore, Missassauga, Ontario, Canada). The multielement solutions containing the matrix elements (0.2 M Na, K, Cs, I or Cl) were prepared from $NaNO_3$ solid (AnalaR, BDH Inc., Toronto, Ontario, Canada), $CsNO_3$ solid (99.999% metals basis, Alfa Aesar, Johnson Matthey, Ward Hill, MA, USA), 10 000 g ml^{-1} K monoelement solution (Plasma Standard from SPEX Industries, Edison, NJ, USA), high-purity HI (Aldrich Chemical Co., Milwaukee, WI, USA) and high-purity HCl (Seastar Chemicals Inc., Sidney, B.C., Canada), respectively. Care was taken to ensure that the counter ion of the matrix element was common to HNO_3 (i.e. either NO_3^- or H^+), so that its effect could be neglected. Indeed, an additional 0.02 M NO_3^- or H^+ should be fairly negligible compared to the 0.16 M already present from 1% HNO_3.

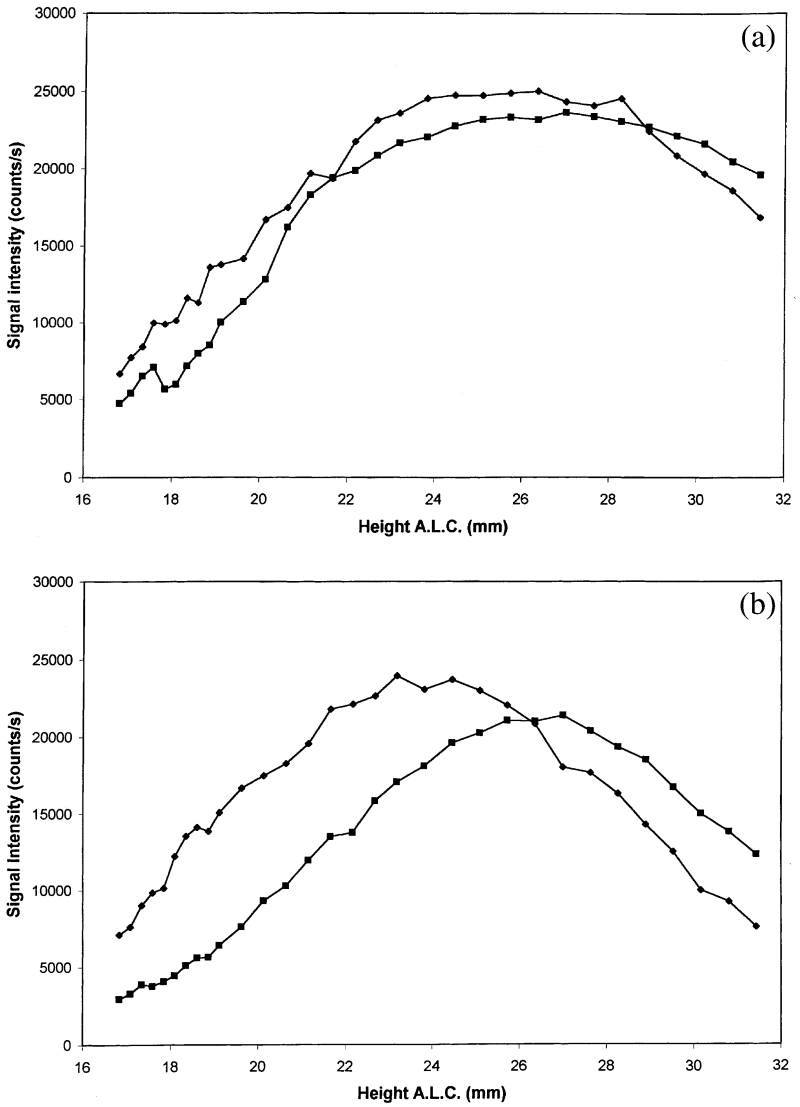

Fig. 4. Axial profiles of the Ar_2^+ signal at m/z 76 with 1% HNO_3 (losanges) and a 0.02-M matrix (squares) being nebulized: (a) Na; (b) K; (c) Cl; and (d) I.

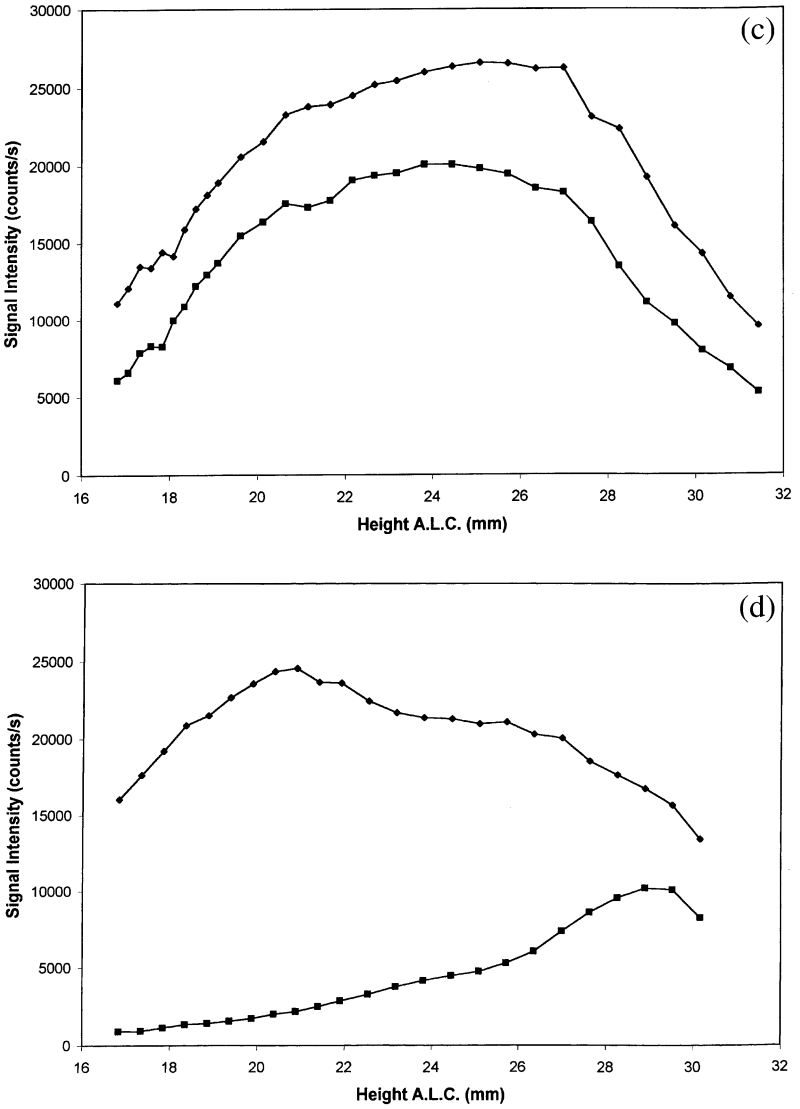

Fig. 4. (*Continued*).

2.3. Procedure

The procedure was identical to that described in Part 1 [1]. Briefly, for each of the concomitant elements (Na, K, Cs, Cl and I), four experiments were carried out, each consisting of four repetitions: (1) the matrix-free multielement solution; (2) a 1% HNO_3 blank; (3) the matrix-containing multielement solution; and (4) a matrix-containing blank in 1% HNO_3. The matrix-free multielement solution was repeated for every experiment in order to account for day-to-day variability in sensitivity. The four experiments consisted of: (1) moving the torch away from the sampler along the central axis of the plasma to get a measurement of the signal intensity at a variety of sampling depths; (2) moving the torch across the sampler at each of three fixed sampling depths (17.5-, 20.0- and 22.5-mm A.L.C., respectively), to get a radial signal profile of the ion distribution

across the central channel of the plasma. Ten replicates were taken at each measurement increment before advancing to the next point of interest.

2.4. Data processing

Microsoft Excel was used to average the replicates and for blank subtraction, where appropriate. Scaling was also done to compensate for day-to-day variations in the instrument response using the matrix-free multielement solution [1].

2.5. Determination of the nebulization efficiency

A custom-made glass tube with a ball joint was used to determine the percentage of nebulized solution exiting the spray chamber. The end of this tube was packed with glass wool and the remainder filled with freshly dried self-indicating silica gel. The gel was packed by lightly tapping the top end of the tube, before being weighed on an analytical balance. The tube was then attached to the exit of the spray chamber (instead of the torch) for approximately 180 s while the solutions were aspirated normally. The tube was immediately weighed upon removal. The increase in weight was then divided by the mass of the nebulized solution to calculate the nebulization efficiency. The mass of nebulized solution was obtained from the change in mass, before and after the solution was aspirated for 180 s, of a small 5-ml beaker filled with solution. This mass was corrected for the different densities of the matrix solutions. This procedure was repeated up to 12 times for each matrix. Between each replicate, the silica gel was discarded and the tube cleaned.

3. Results and discussion

3.1. Analyte oxides

The signal of the LaO^+ and CeO^+ appears distinctly sooner in the plasma (i.e. at a smaller sampling position) than that of the corresponding analytes (as can be seen in Fig. 1a, where La is contrasted to Pb, an element that does not form a refractory oxide), which is in agreement with what has been seen before [12,14]. The oxides are formed at low heights A.L.C. where the plasma is somewhat cooler [12]. As they are carried to greater heights A.L.C., they are then dissociated into their respective analytes, which results in the

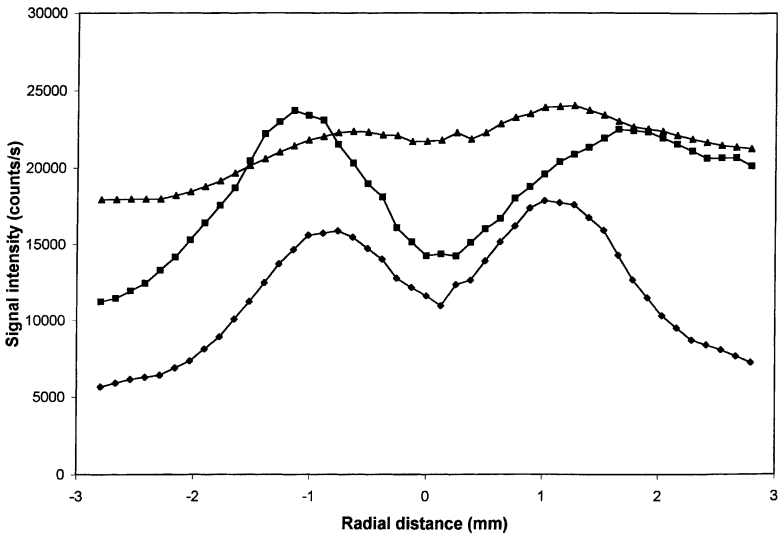

Fig. 5. Radial profiles of the Ar_2^+ signal at m/z 76 with 1% HNO_3 being nebulized at three different heights A.L.C.: (a) 17.5 (losanges); (b) 20.0 (squares); and (c) 22.5 mm (triangles).

analyte signal intensity increasing with sampling distance. When the bulk of the LaO^+ species have been dissociated, the La^+ analyte signal then begins to decrease with increasing height A.L.C. as is normal. Fig. 1b shows the combined signals for both species of the element (La^{2+} was not included because its signal intensity is smaller than the error on the signal intensity of the other ions) in comparison to Pb, an element which does not easily form an oxide. It clearly shows that the total signal due to a particular analyte is very similar whether or not the analyte forms an oxide. Fig. 2 demonstrates that this is still true when a matrix element (in this example, Na) is present.

However, comparison of Fig. 2 to Fig. 1b reveals a shift to lower heights A.L.C. in presence of the 0.02 M Na matrix. In part 1 of this study, this shift was attributed to a combination of earlier desolvation and a shift in the atom-ion equilibrium [1]. If this is indeed the case, a change

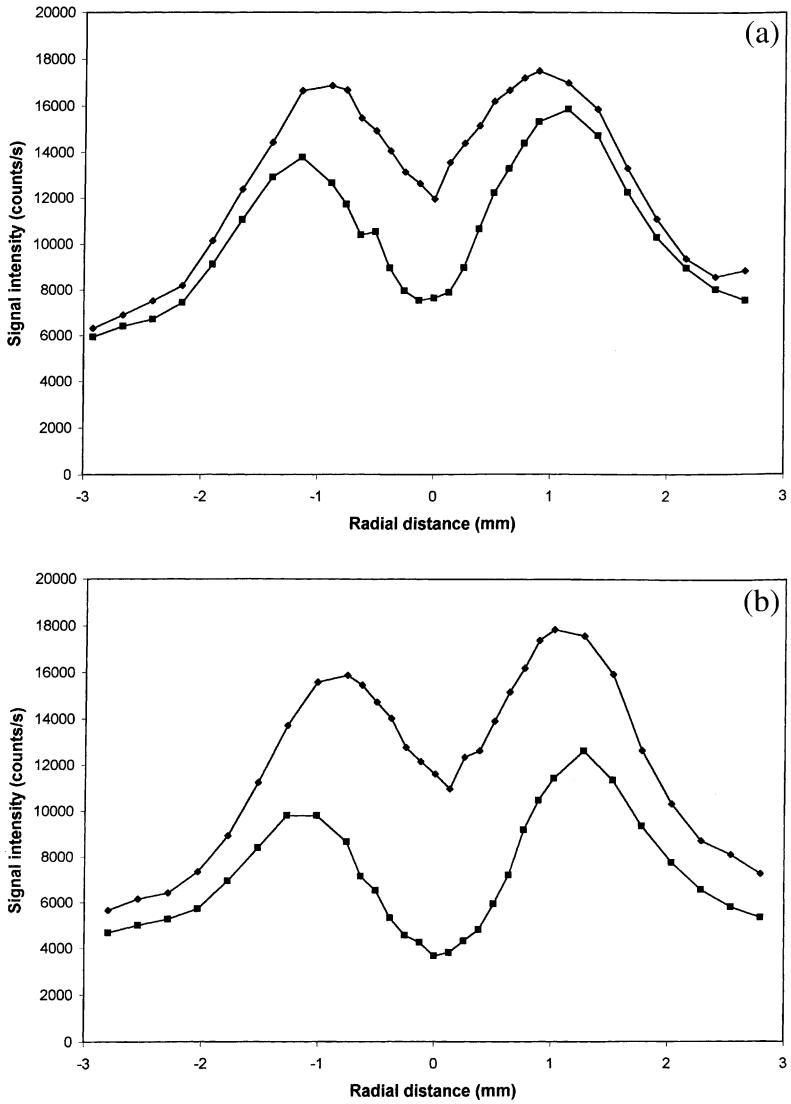

Fig. 6. Radial profiles of the Ar_2^+ signal at m/z 76 with 1% HNO_3 (losanges) and a 0.02-M matrix (squares) being nebulized: (a) Na; and (b) K.

should be expected in the $MO/(M + MO)$ profile [8]. Fig. 3 shows the axial profiles of the $LaO^+/(La^+ + LaO^+)$ ratio obtained in the various matrices (as for all the other figures, similar profiles were obtained for Ce). Clearly, only the E.I.E.s had an effect on the profile. Indeed, the profiles with or without 0.02 M Cl or I are essentially identical. Furthermore, these differences cannot be attributed to a change in nebulization efficiency since all matrix solutions, except that of Na, resulted in the same nebulization efficiency as shown in Table 1.

However, an earlier desolvation would be expected to shift the whole profile to lower height A.L.C.. On the other hand, a shift in the ionization equilibrium would only affect the region where the electron population is significantly changed, i.e. at low heights A.L.C., where suppression may be expected. The latter is clearly observed in the presence of 0.02 M Na where the

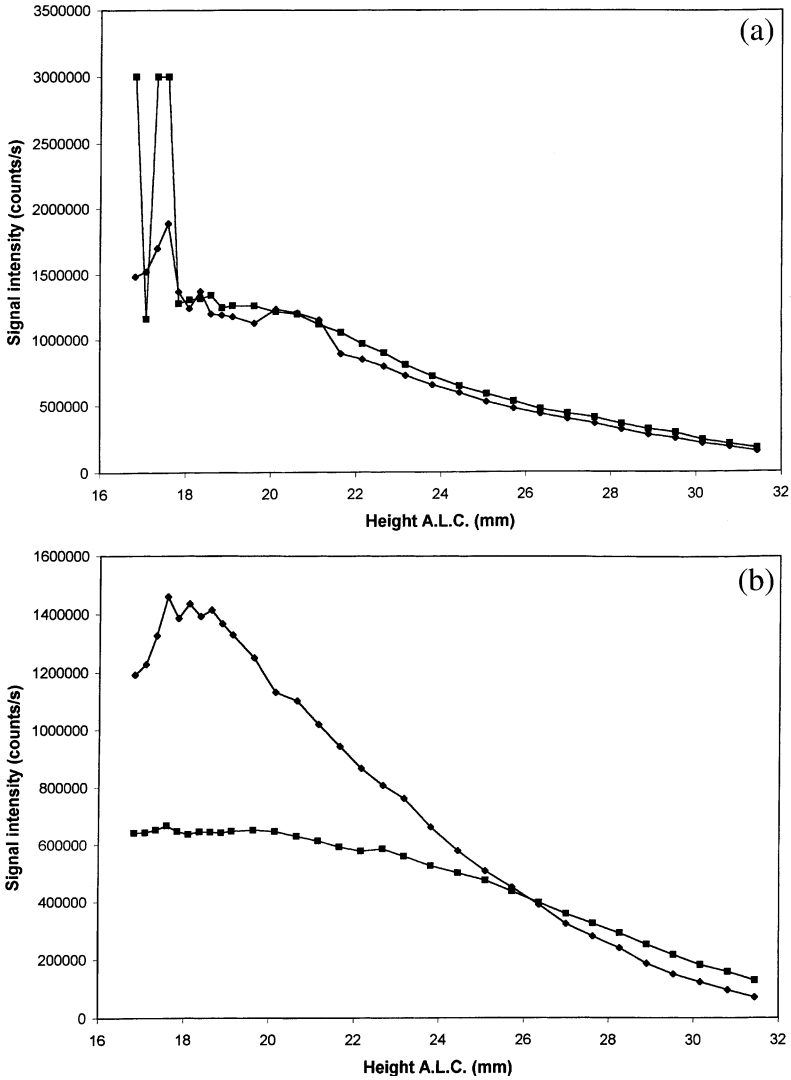

Fig. 7. Axial profiles of the ArO^+ signal at m/z 56 with 1% HNO_3 (losanges) and a 0.02-M matrix (squares) being nebulized: (a) Na; (b) K; (c) Cl; and (d) I.

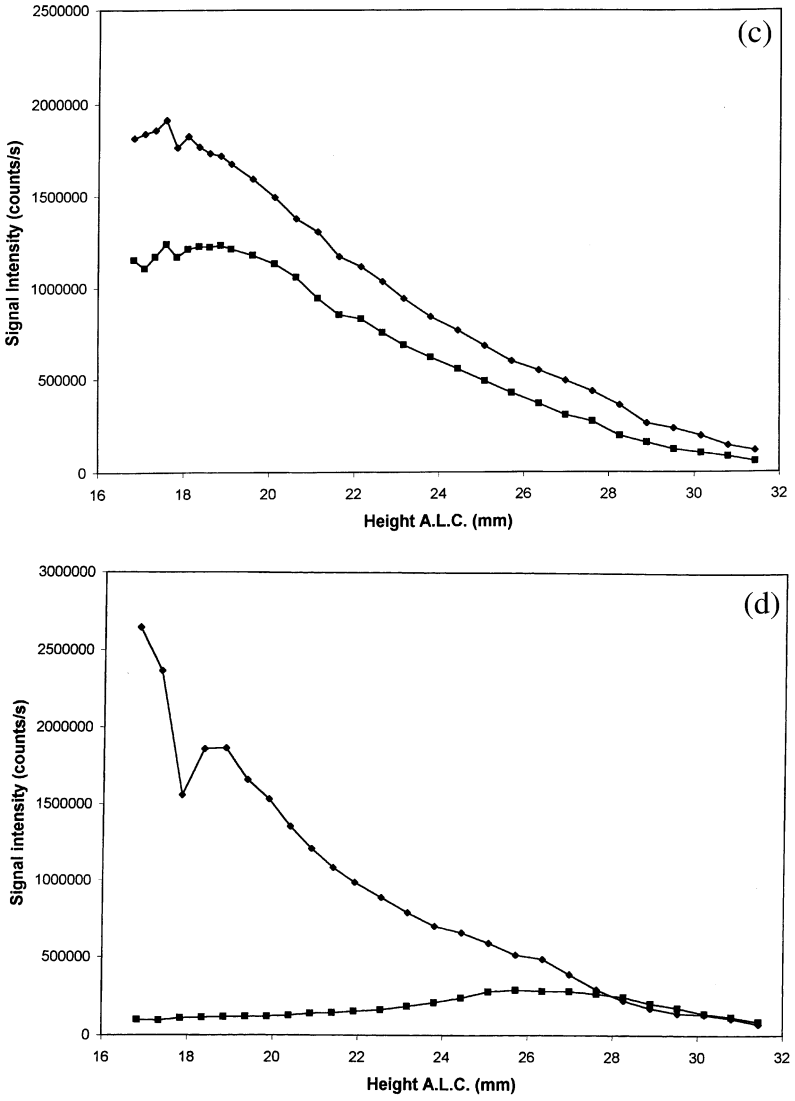

Fig. 7. (*Continued*).

profiles are essentially identical, except at low heights A.L.C. The oxide ratio profile therefore suggests that a shift in the ionization equilibrium mainly occurs in this matrix. In the case of K and Cs, a shift of the whole profile is clearly observed, consistent with earlier desolvation. The shift is so important that it would likely mask changes induced by any shift in ionization equilibrium.

3.2. Ar_2 at m/z 76

The Ar_2^+ signal at *m/z* 76 may allow some insight into the migration of Ar^+ ions and neutrals from the bulk plasma gas into the central axis. Furthermore, this signal should be independent of changes in desolvation rate and should therefore, provide further evidence in shift in the

ionization equilibrium. This polyatomic ion has also been used as an internal standard [22], so its behavior in the presence of a matrix element has a practical significance.

3.2.1. Axial profiles

Fig. 4a shows that the Ar_2^+ signal at m/z 76 is weak at low sampling heights in the plasma and rises in strength with increasing sampling height until it reaches a peak at approximately 25 mm A.L.C. The signal then decreases steeply to the extent of the observed region. The addition of a matrix element shifts the signal of this polyatomic ion similarly to what was described in part 1 for the analytes, however, the suppression is, in general, more severe.

In the presence of a 0.02-M Na matrix, the signal is slightly suppressed and the maximum is somewhat shifted to a greater height A.L.C. (Fig. 4a), which is consistent with a shift in ionization

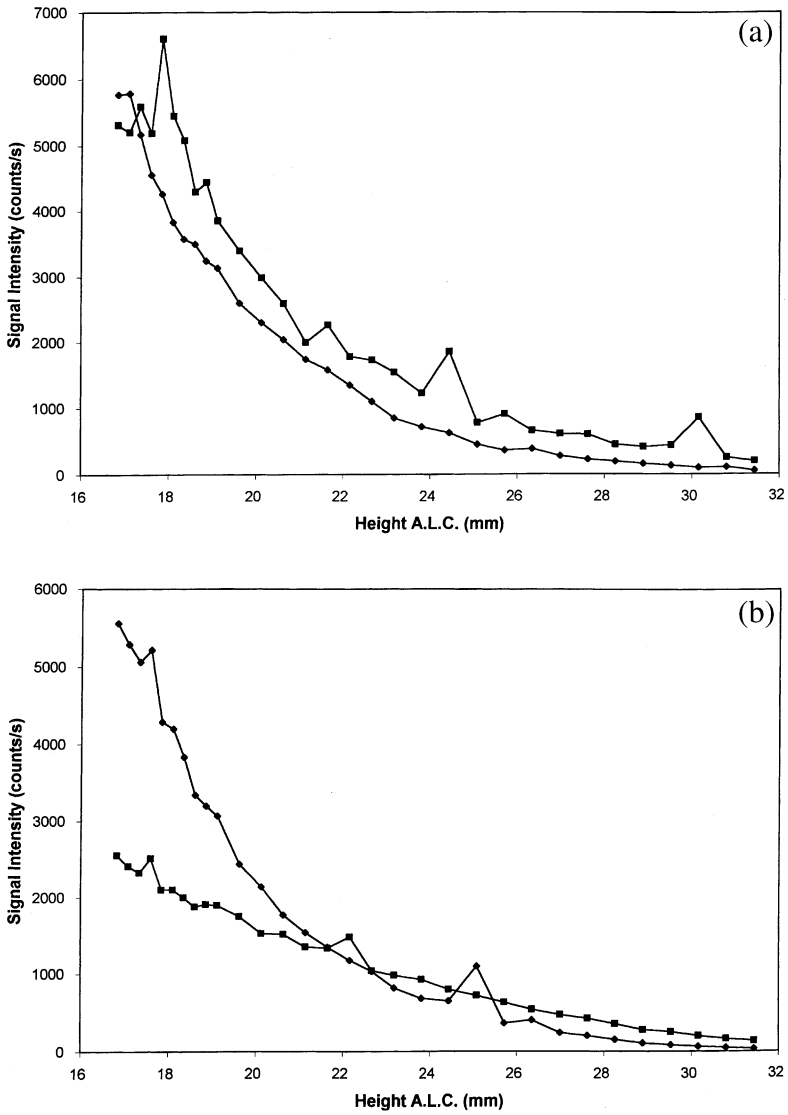

Fig. 8. Axial profiles of the CO_2^+ signal at m/z 48 with 1% HNO_3 (losanges) and a 0.02-M matrix (squares) being nebulized: (a) Na; (b) K; and (c) Cl.

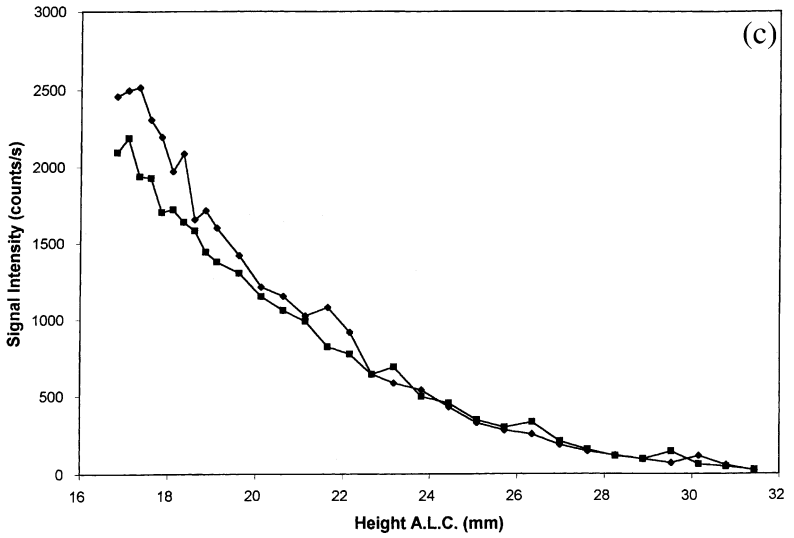

Fig. 8. (*Continued*).

equilibrium. A 0.02-M K matrix shifts the signal significantly to a greater height A.L.C. (Fig. 4b), again consistent with a shift in the ion–atom equilibrium. The more significant shift observed with K is likely due to concurrent space–charge effects. The latter are indeed expected to be more important for K than Na.

The addition of a 0.02-M Cl matrix does not shift the location of the signal intensity maximum. However, there is a larger suppression than that seen in the presence of K and the degree of suppression is similar over the whole observed region (Fig. 4c). This is likely the result of the competing collision-induced formation of $ArCl^+$, which has been reported to occur in the interface region [15,16]. Iodine suppresses the signal very heavily close in to the load coil before the signal rises to a maximum at approximately 30 mm A.L.C. (Fig. 4d). A greater suppression also occurred in 0.02 M Cs (not shown). This great suppression is clearly consistent with space–charge effects with the I and Cs matrices.

Nonetheless, from Fig. 4, it is apparent that Ar_2^+ is affected differently than the analyte elements by the presence of a matrix element. The same general patterns of suppression are followed, i.e. Cs > I > K > Cl similarly to the analytes, however, the exact degree of suppression is significantly different than that seen for almost all of the analytes (most notably ^{75}As.) The major exception is in the presence of the Cs matrix where Ar_2^+ is suppressed to the same extent as the bulk of the analytes.

3.2.2. Radial profiles

The radial profiles for Ar_2^+ have a very distinctive 'seagull' shape (Fig. 5). The profile is roughly symmetrical along the central axis. The signal rises from above background levels at the edges of the observed region similarly to the analyte profiles, but then reaches a maximum and descends through a local minimum along the central axis. This minimum is at an intensity of approximately two-thirds that at the maxima on either side. The signal intensity along the central axis becomes stronger with increasing sampling distance and the central depression becomes less pronounced.

The addition of a matrix element changes the radial profiles. At 17.5 mm A.L.C., the signal is slightly suppressed at the edges and more heavily suppressed along the central axis (Fig. 6). This occurs for all of the matrix elements. The degree of this suppression is dependent upon which ma-

trix element is present, following the same patterns that have been described for the analytes in part 1 [1].

The radial profiles reveal that as the distance from the torch increases, the Ar^+ ion diffuses into the central channel (Fig. 5). This diffusion is counteracted or delayed by the presence of a matrix ion. The suppression of Ar_2^+ at m/z 76 is strongly related to matrix element mass since a linear regression between the percentage of signal suppression and the matrix element mass yields a correlation coefficient of 0.99, which indicates space–charge effects.

3.3. ArO at m/z 56

Graphs of the axial profiles show that ArO^+ is suppressed more heavily in the presence of the

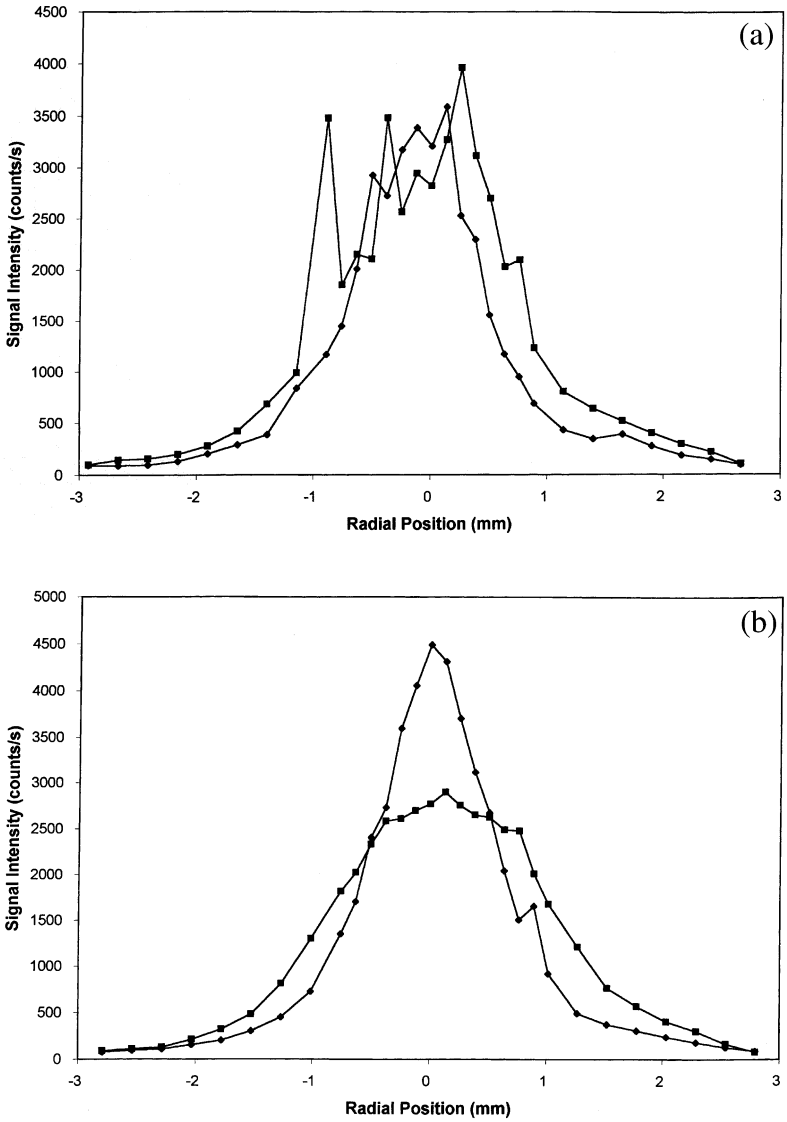

Fig. 9. Radial profiles of the CO_2^+ signal at m/z 48 with 1% HNO_3 (losanges) and a 0.02-M matrix (squares) being nebulized: (a) Na; and (b) K.

non-E.I.E. elements than the other analyte elements (Fig. 7). In the presence of the E.I.E.s, the suppression is less than that seen for the analytes in part 1 [1], while for the non-E.I.E.s, it is greater than that of the analytes. Radial profiles support what was seen in the axial profiles. The non-E.I.E. matrix elements have a greater effect upon the $^{56}ArO^+$ signal than the E.I.E. elements when compared to their effect upon the analytes. The suppression of $^{56}ArO^+$ is more strongly correlated with matrix element mass than the analytes, with a correlation coefficient of 0.98 at the height of maximum signal, very similar to that of $^{76}Ar_2^+$. This is consistent with space–charge effects.

3.4. CO_2 at m/z 48

The axial profiles show some similarities to those of the analyte elements, with the exception of the 0.02-M Na matrix that results in a slight enhancement at all heights A.L.C. (Fig. 8a). In the presence of 0.02 M K, the signal is first suppressed and then becomes slightly enhanced at approximately 21 mm A.L.C. (Fig. 8b). As has been seen for all of the other signals, 0.02 M Cs suppresses the signal completely at all heights A.L.C. The addition of Cl results in a slight suppression at closer sampling distances (closer than 22.5 mm A.L.C.) and no change above this height (Fig. 8c). The I matrix suppresses the signal heavily over most of the profile but this eventually switches to an enhancement at approximately 27.5 mm A.L.C.

The radial profiles also show similarities to those of the analytes. With 0.02 M Na, the profiles are quite noisy, but exhibit some broadening of the signal, most notably at 17.5 mm A.L.C., the lowest height profiled (Fig. 9a). The profiles with 0.02 M K show even more broadening (Fig. 9b), which may be further evidence of ambipolar diffusion. The Cs matrix totally suppresses the signal along the central axis as expected. In the presence of a Cl matrix, the signal is slightly suppressed along the central axis, but is unaffected otherwise. The I matrix suppresses the signal heavily at all radial positions.

These observations indicate that CO_2^+ behaves quite similarly to the analyte ions. However, its suppression is more strongly correlated with the mass of the matrix ion (the correlation coefficient is 0.88) than that of most of the analytes.

4. Conclusions

Although space–charge effects are in general dominant, this study has revealed further evidence for a shift in ionization equilibrium being a significant source of non-spectroscopic interference in the presence of E.I.E.s. This was particularly evident with Na, an element which is not expected to induce significant space–charge effects, at least not at the 0.02 M level. Not only do E.I.E.s shift the Ar_2^+ profile to greater height A.L.C., but they also changed the $MO^+/(MO^+ + M^+)$ at low heights A.L.C. Evidence for an earlier desolvation was observed in the $MO^+/(MO^+ + M^+)$ axial profiles in presence of K and Cs, where the whole profile was shifted to lower height A.L.C. This study also showed that CO_2^+, a background ion originating from the sample, behaved similarly to the analytes. However, its use as an internal standard is precluded by the fact that its signal is very weak and suffers from considerable noise due to background signals.

Acknowledgements

The authors are grateful to Perkin–Elmer for the donation of ELAN 5000 software, to Dr Conrad Grégoire for the donation of samplers and skimmers, and to Robert Campbell for repairing the occasionally melted torch. M.F. is thankful for the financial support from the Queen's School of Graduate Studies and the Association of Official Analytical Chemists. D.B. gratefully acknowledges funding from the Natural Sciences and Engineering Research Council of Canada (through Grant no. OGP0039487).

References

[1] M.M. Fraser, D. Beauchemin, Effect of concomitant elements on the distribution of ions in ICP-MS. Part 1. elemental ions, Spectrochim. Acta Part B 55 (2000) 1705–1731.

[2] J.A. Olivares, R.S. Houk, Suppression of analyte signal by various concomitant salts in inductively coupled plasma mass spectrometry, Anal. Chem. 58 (1986) 20–25.
[3] C. Vandercasteele, M. Nagels, H. Vanhoe, R. Dams, Suppression of analyte signal in inductively-coupled plasma/mass spectrometry and the use of an internal standard, Anal. Chim. Acta 211 (1988) 91–98.
[4] A.C. Lazar, P.B. Farnsworth, Matrix effect studies in the inductively coupled plasma with monodisperse droplets – part II influence of matrix on spatially integrated ion density, Appl. Spectrosc. 53 (1999) 465–470.
[5] Q. Xu, G. Mattu, G.R. Agnes, Influence of droplets with net charge in inductively coupled plasma atomic emission spectroscopy and implications for the easily ionizable element chemical matrix effect, Appl. Spectrosc. 53 (1999) 965–973.
[6] J.Q. Xu, D. Balik, G.R. Agnes, Aerosol static electrification and its effects in inductively coupled plasma spectroscopy, J. Anal. At. Spectrom. 16 (2001) 715–723.
[7] D.S. Hanselman, N.N. Sesi, M. Huang, G.M. Hieftje, The effect of sample matrix on electron density, electron temperature and gas temperature in the argon inductively coupled plasma examined by Thomson and Rayleigh scattering, Spectrochim. Acta Part B 49 (1994) 495–526.
[8] S.D. Tanner, ICP-MS tectonics: moving the atomic and oxide ion 'mountains', paper F1. Proceedings of the 1994 Winter Conference on Plasma Spectrochemistry, San Diego, January 1994.
[9] M.A. Vaughan, G. Horlick, Effect of sampler and skimmer orifice size on analyte and analyte oxide signals in inductively coupled plasma mass spectrometry, Spectrochim. Acta Part B 45 (1990) 1289–1299.
[10] S.E. Hobbs, J.W. Olesik, Inductively coupled plasma mass spectrometry signal fluctuations due to individual aerosol droplets and vaporizing particles, Anal. Chem. 7 (1992) 275–283.
[11] S.E. Hobbs, J.W. Olesik, The effect of desolvating droplets and vaporizing particles on ionization and excitation in Ar inductively coupled plasmas, Spectrochim. Acta Part B 48 (1993) 817–833.
[12] E. Poussel, J.-M. Mermet, D. Deruaz, Dissociation of analyte oxide ions in inductively coupled plasma mass spectrometry, J. Anal. Atom. Spectrom. 9 (1994) 61–66.
[13] S.D. Tanner, Experimental studies of ion kinetic energies in ICP-MS, in: G. Holland, A.N. Eaton (Eds.), Applications of Plasma Source Mass Spectrometry II, Special Publication No. 124, Royal Society of Chemistry, Cambridge, 1993, pp. 222–234.
[14] G.H. Vickers, D.A. Wilson, G.M. Hieftje, Spatial dependence of ion concentrations in inductively coupled plasma mass spectrometry, Spectrochim. Acta Part B 45 (1990) 499–509.
[15] N. Nonose, M. Kubota, Non-spectral and spectral interferences in inductively coupled plasma high-resolution mass spectrometry — part I. Optical characteristics of micro-plasmas observed just behind the sampler and the skimmer in inductively coupled plasma high resolution mass spectrometry, J. Anal. At. Spectrom. 16 (2001) 551–559.
[16] N.S. Nonose, N. Matsuda, N. Fudagawa, M. Kubota, Some characteristics of polyatomic ion spectra in inductively coupled plasma mass spectrometry, Spectrochim. Acta Part B 49 (1994) 955.
[17] T.J. Cleland, F.R. Meeks, Statistical mechanics of Ar^{2+} in an inductively coupled plasma, Spectrochim. Acta Part B 51 (1996) 1487–1490.
[18] S.D. Tanner, Characterization of ionization and matrix suppression in inductively coupled 'cold' plasma mass spectrometry, J. Anal. At. Spectrom. 10 (1995) 905–921.
[19] D.C. Harris, Quantitative Chemical Analysis, 5th ed, W.H. Freeman and Company, New York, 1999, p. 136.
[20] J.W. Moore, C.L. Stanitski, J.L. Wood, J.C. Kotz, M.D. Joesten, The Chemical World, Concepts and Applications, 2nd ed, Harcourt Brace and Company, Florida, 1998, p. 467.
[21] E. Björn, W. Frech, Non-spectral interference effects in inductively coupled plasma mass spectrometry using direct injection high efficiency and microconcentric nebulisation, J. Anal. Atom. Spectrom. 16 (2001) 4–11.
[22] D. Beauchemin, J.W. McLaren, S.S. Berman, Study of the effects of concomitant elements in inductively coupled plasma mass spectrometry, Spectrochim. Acta Part B 42 (1987) 467–490.